

Electronic supplementary information (ESI)

Polyhedral Oligomeric Silsesquioxane Functionalized Copper Trimesate

E. S. Sanil,^{a,b} Kyung-Ho Cho,^a Do-Young Hong,^{a,b} Ji Sun Lee,^a Sukyung Lee,^a Sam Gon Ryu,^d Hae Wan Lee,^d Jong-San Chang,^{a,c} Young Kyu Hwang^{a,b*}

^aCatalysis Center for Molecular Engineering (CCME), Korea Research Institute of Chemical Technology (KRICT), Shinseongno 17, Yuseong, Daejeon 305-600, Korea, E-mail: ykhwang@kRICT.re.kr

^bDepartment of Green Chemistry, University of Science and Technology (UST), 217 Gajeong-Ro, Yuseong, Daejeon 305-350, Korea

^cDepartment of Chemistry, Sungkyunkwan University, Suwon 440-476, Korea

^dAgency for Defense Development, Yuseong P.O. box 35-52, Daejeon 305-600, Korea

All reagents, Copper (II) acetate monohydrate (TCI), Benzene- 1, 3, 5-tricarboxylic acid (Aldrich), dodecanoic acid (Aldrich), 1- Butanol (Aldrich), Potassium sulphate (Aldrich), Amino propyl isooctyl polyhedral silsesquioxane (Hybrid plastics USA) were used as purchased without further purification.

Synthesis of $\text{Cu}_3(\text{BTC})_2$ by microwave assisted coordination modulation method

In a typical experiment, copper acetate monohydrate ($\text{Cu}(\text{OAc})_2 \cdot \text{H}_2\text{O}$; 0.17 mmol) and dodecanoic acid (4.7 mmol) were dissolved in 1-butanol (7.76 mmol) in a Teflon vessel. The mixture was quickly heated with a heat gun to obtain a clear solution. Benzene- 1, 3, 5-tricarboxylic acid (0.095 mmol) was added at room temperature, and the sealed reaction mixture was placed in the microwave reactor and heated to 140 °C for 15 min. The resulting blue powder was isolated by centrifugation and washed with ethanol by three dispersion-sonication-centrifugation cycles. The resulting light blue solid was purified by soaking in ethanol at 70 °C for 12 hours. After methanol soaking was filtered and dried for 12 hour at 100 °C.

Modification of $\text{Cu}_3(\text{BTC})_2$ with Amino propylisooctyl polyhedral silsesquioxane (O-POSS).

About 1g $\text{Cu}_3(\text{BTC})_2$ was activated by heating at 150 °C under vacuum. Activated $\text{Cu}_3(\text{BTC})_2$ was then mixed with a solution of Amino propyl isooctyl polyhedral silsesquioxane (0.25g) in 60 mL n-hexane in a 100 mL two neck RB and refluxed under flowing nitrogen for 48 h. After reflux, filtered and washed with large amount of hexane and was dried at at 100 °C for 12 h.

Characterization

The as-synthesized $\text{Cu}_3(\text{BTC})_2$ and $\text{O-POSS@Cu}_3(\text{BTC})_2$ materials were characterized for their structural integrities by XRD and SEM. Powder X-ray diffraction patterns of all the samples were recorded by a Rigaku diffractometer (D/MAX IIIB, 2 kW) using Ni-filtered Cu $K\alpha$ -radiation (40 kV, 30mA, $\lambda = 1.5406 \text{ \AA}$) and a graphite crystal monochromator. The crystal sizes and morphology of the materials were examined using a scanning electron microscope (SEM, JEOL JSM-840A) and transmission electron microscope (.TECNAI G2 RETROFTI). Specific surface areas were measured by N_2 adsorption and desorption isotherms at liquid nitrogen temperature using a sorption analyzer (Micromeritics, Tristar 3000) and standard multipoint BET analysis method. Samples were degassed in flowing N_2 for 12 h at $150 \text{ }^\circ\text{C}$ before N_2 physisorption measurements. The specific surface areas were evaluated using the Brunauer-Emmett-Teller (BET) method in the p/p_0 range of 0.05 – 0.2. The pore size distribution was determined using Barrett-Joyner-Halenda (BJH) method and obtained from the analysis of the adsorption branch of the isotherm. Micropore size distribution was determined from Ar sorption technique by using Horvath-Kawazoe method. The metal content in the materials were analysed by ICP-AES technique (Thermo scientific Icap 6500 duo inductively coupled plasma-atomic emission spectrometer). Thermogravimetric (TGA) analysis were carried out under nitrogen (100 mL min^{-1}) with a Perkin-Elmer electrobalance TGA-7 at a heating rate of 5 min^{-1} up to $700 \text{ }^\circ\text{C}$. Before TGA analysis the samples were kept under saturated NH_4Cl atmosphere in a closed chamber for 24 h.

In order to carefully measure change of concentration of CUS, we used amino-5-nitrobenzonitrile (ANB) as an internal standard in which CN band is clearly separated from vibration of CO adsorption. Therefore, we can avoid the tolerance of peak intensity by different thickness of self-supported pellets after normalization of the FT-IR spectra with ANB. ANB

physically mixed with $\text{Cu}_3(\text{BTC})_2$ and $\text{O-POSS@Cu}_3(\text{BTC})_2$, respectively, and the ratio of MOF/ANB was 50. Samples were outgassed at 423 K for 6 h, and then CO gas was introduced at 110K. The FT-IR spectra were measured after an equilibrium pressure of CO (200 Pa). To confirm the physisorption and chemisorptions of CO, the FT-IR spectra were measured under evacuation condition after an equilibrium CO pressure.

Dynamic water adsorption and desorption cycle test

Hydrothermal stability test by water sorption cycling were performed as follows. A humidified nitrogen gas flow (RH 80% H_2O vapor pressure) was maintained through a thermogravimetric balance. The temperature of the sample chamber was changed between 30°C and 100 °C with cycle time of 3h.

Ammonia breakthrough test

To perform the ammonia breakthrough test under 15% RH condition at 25 °C, approximately 0.246 ml of sample with 60-70 mesh particle size was loaded into 3.96 mm i.d quartz tube reactor. Before the breakthrough test for 1st cycle and 2nd cycle, each sample was activated for 6h at 150 °C under 20ml/min He flow. The concentration of the mixed ammonia/Air balanced gas was 1000 ppm and flow rate was 43.6 ml/min. Linear velocity (cm/s) and residence time (sec) of ammonia gas mixture were 5.9 cm/s and 0.339 sec respectively. Before testing for the humidity condition, each sample was exposed to 15 % RH air stream for 2hr. During the breakthrough test for ammonia, the concentration of effluent gas was recorded with tuneable diode laser NH_3 gas detector. The amounts of adsorbed NH_3 were calculated by the integration of breakthrough curve for sample subtracted with the integration of breakthrough curve for blank test. As reported in the previous literature [1], the main site of absorption of the ammonia gas in the $\text{Cu}_3(\text{BTC})_2$

framework is copper dimer that can provide Lewis acid sites by the activation step and 1 mol of copper dimer was known to provide irreversible chemisorption sites for 2mole of NH₃.¹ In the case of O-POSS@Cu₃(BTC)₂ framework, some part of copper dimer was already coordinated to amine functionality in the O-POSS, which strongly bound to copper metal site up to 350 °C as shown to be TGA result(see Figure S3) so that the less amount of usability for copper metal site was offered to NH₃.

Reference

1. J. B. Decoste and G. W. Peterson, *Chem. Rev.*, 2014, **114**, 5695.

Table S1 Texture properties and the results of NH₃ breakthrough tests at dry and 15 % RH condition of Cu₃(BTC)₂ and O-POSS@Cu₃(BTC)₂

Material	Surface area (BET) (m ² /g)	Total pore volume (cm ³ /g)	Metal content ICP (wt%)		NH ₃ sorption condition	Adsorbed amount of NH ₃ (mmol/g sorbent)
			Cu	Si		
Cu ₃ (BTC) ₂	1661	0.57	22.3		15	7.51
					(Reactivated)15	4.45
O-POSS@Cu ₃ (BTC) ₂	1514	0.55	25.1	1.39	15	7.35
					(Reactivated)15	5.06

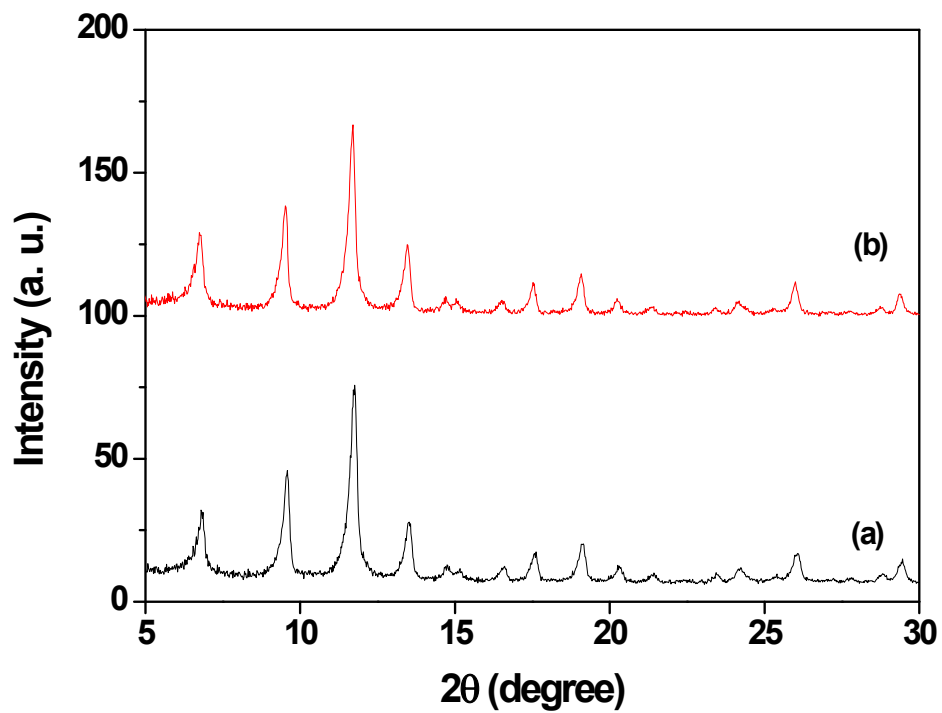


Figure S1 XRD patterns of (a) $\text{Cu}_3(\text{BTC})_2$ and (b) $\text{O-POSS@Cu}_3(\text{BTC})_2$

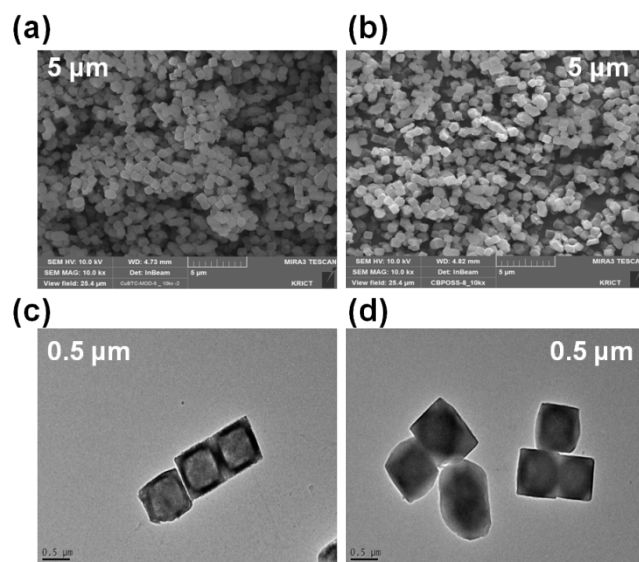


Figure S2 SEM (a and b) and TEM (c and d) images of $\text{Cu}_3(\text{BTC})_2$ and $\text{O-POSS@Cu}_3(\text{BTC})_2$ respectively.

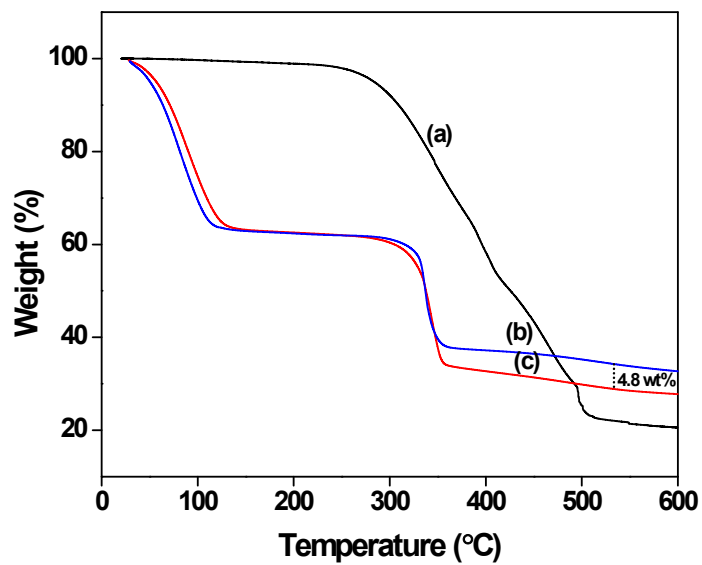


Figure S3 TGA patterns of (a) O-POSS (b) $\text{Cu}_3(\text{BTC})_2$ and (c) O-POSS@ $\text{Cu}_3(\text{BTC})_2$.

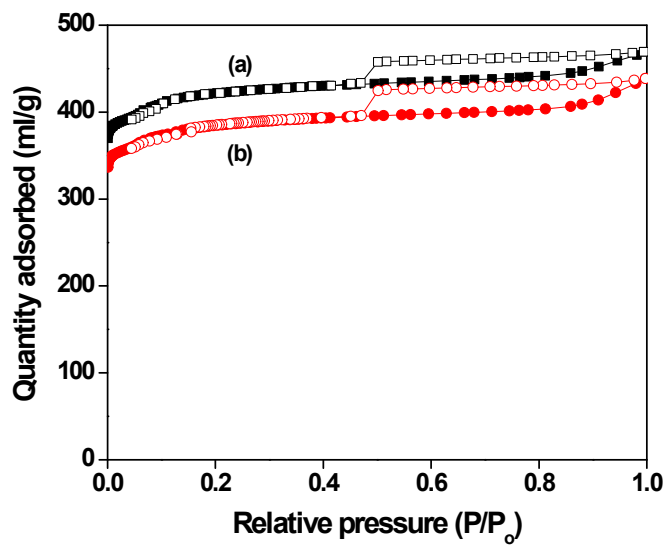


Figure S4 N_2 sorption isotherms of (a) $\text{Cu}_3(\text{BTC})_2$ and (b) O-POSS@ $\text{Cu}_3(\text{BTC})_2$.

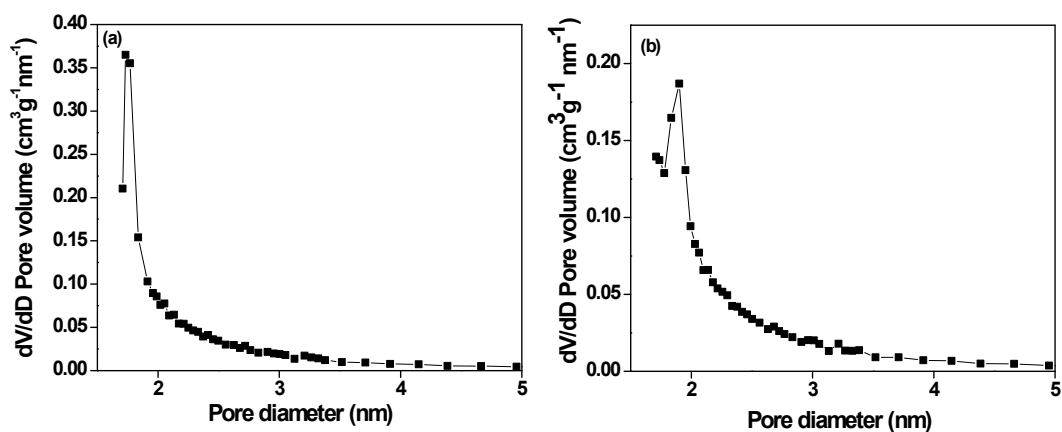


Figure S5 BJH pore size distribution of (a) $\text{Cu}_3(\text{BTC})_2$ and (b) $\text{O-POSS}@Cu_3(\text{BTC})_2$. (N_2 sorption)

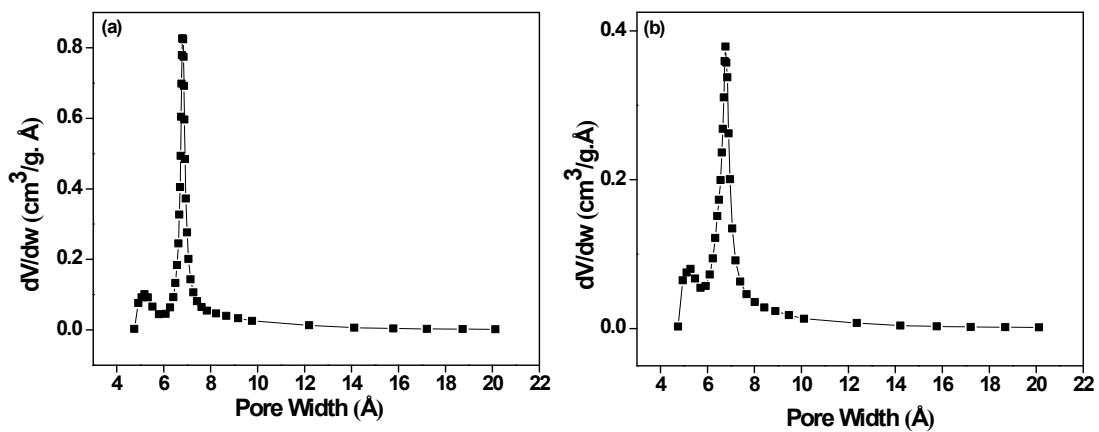


Figure S6 Horvath-Kawazoe micropore size distribution of (a) $\text{Cu}_3(\text{BTC})_2$ and (b) $\text{O-POSS}@Cu_3(\text{BTC})_2$ (Ar sorption).

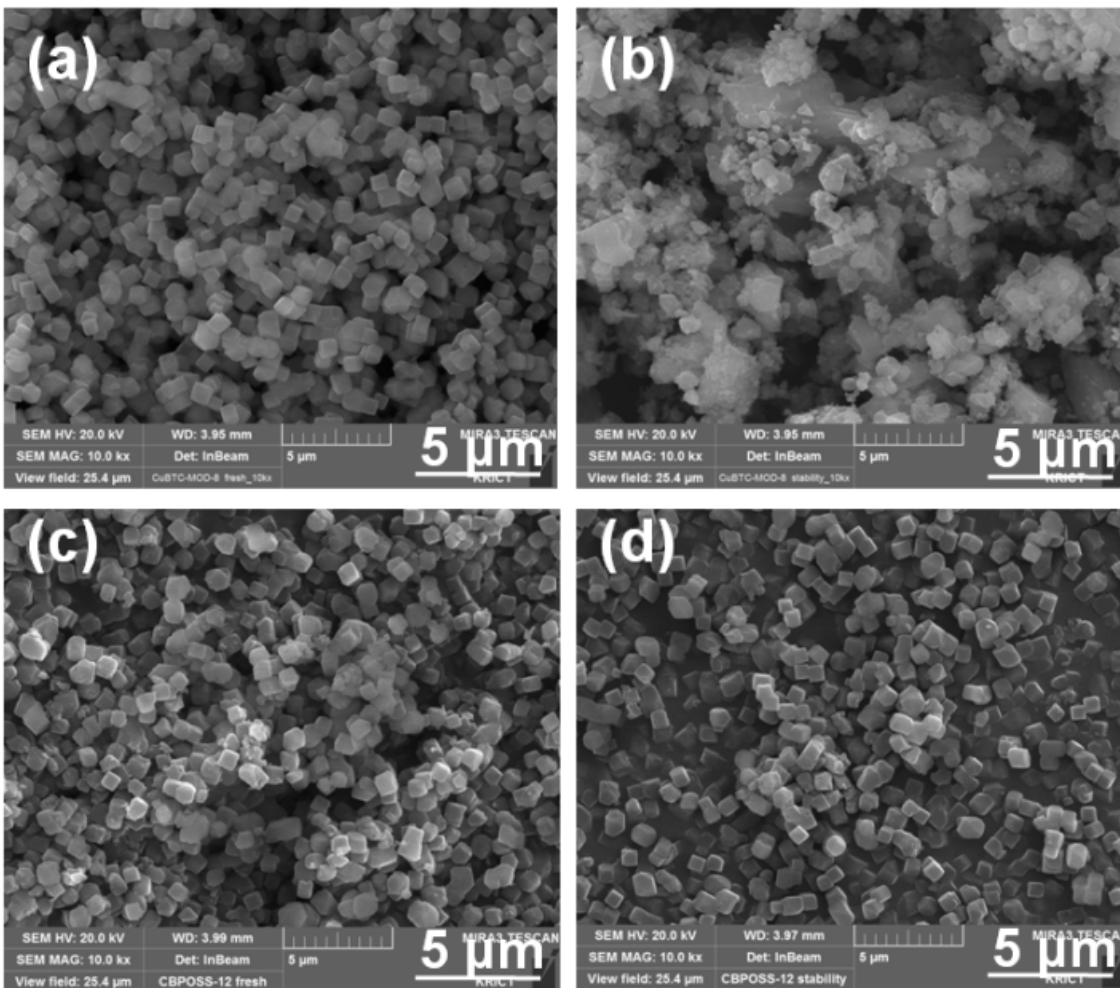


Figure S7 SEM images of $\text{Cu}_3(\text{BTC})_2$ and $\text{O-POSS}@\text{Cu}_3(\text{BTC})_2$, fresh (a and c) and after exposure to 90 % RH (b and d) at room temperature for 1 week under saturated K_2SO_4 solution atmosphere respectively.

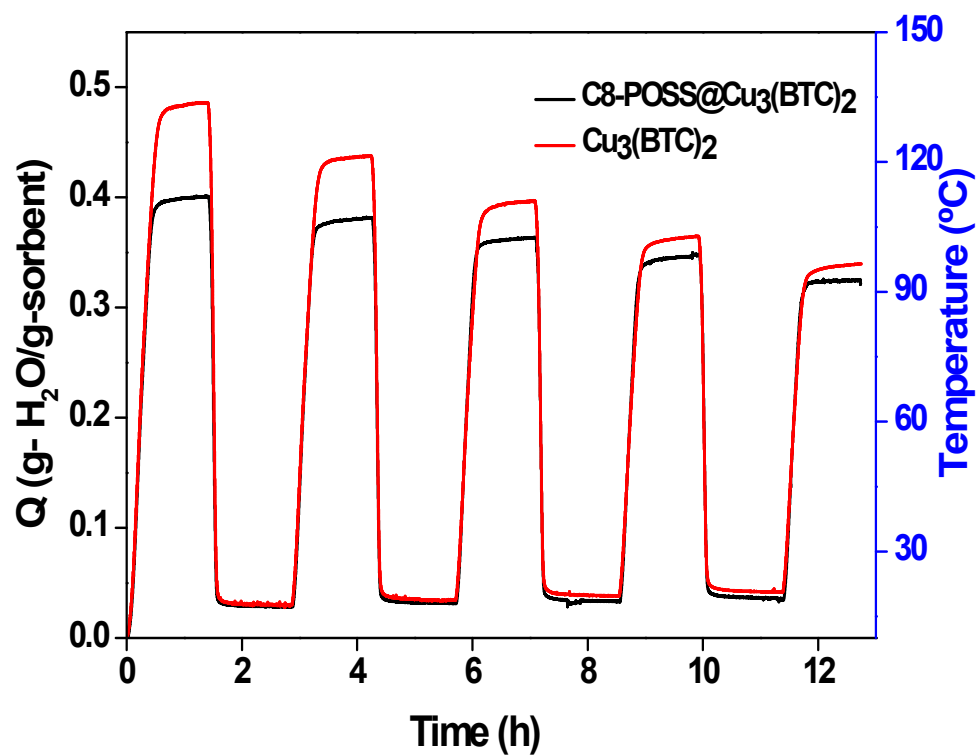


Figure S8 Dynamic water adsorption and desorption cycle tests of Cu₃(BTC)₂ and O-POSS@Cu₃(BTC)₂

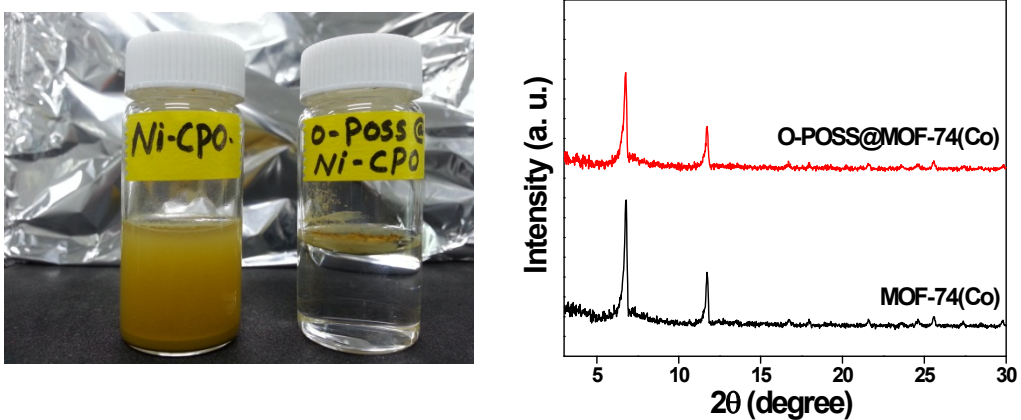


Figure S9. Photo images of CPO-27(Ni) (left) in water and XRD patterns (right) of (a) MOF-74(Co)

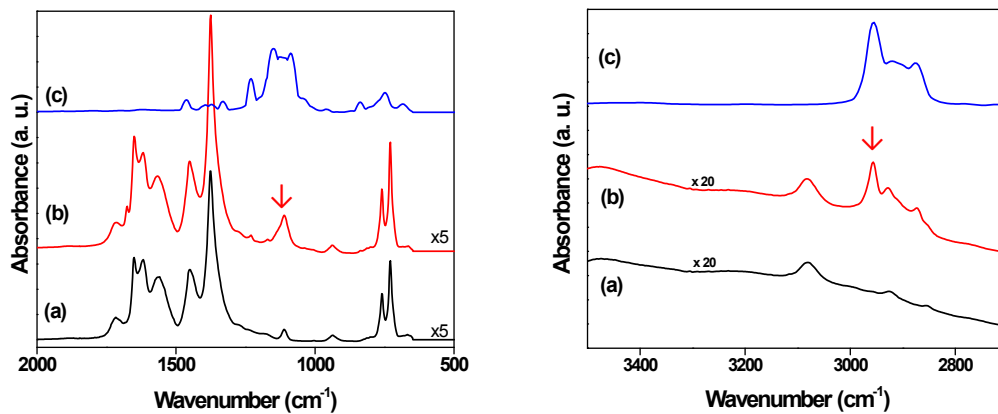


Figure S10. FT-IR spectra of (a) $\text{Cu}_3(\text{BTC})_2$, (b) $\text{O-POSS@Cu}_3(\text{BTC})_2$, and (C) O-POSS , kept at 298 K.

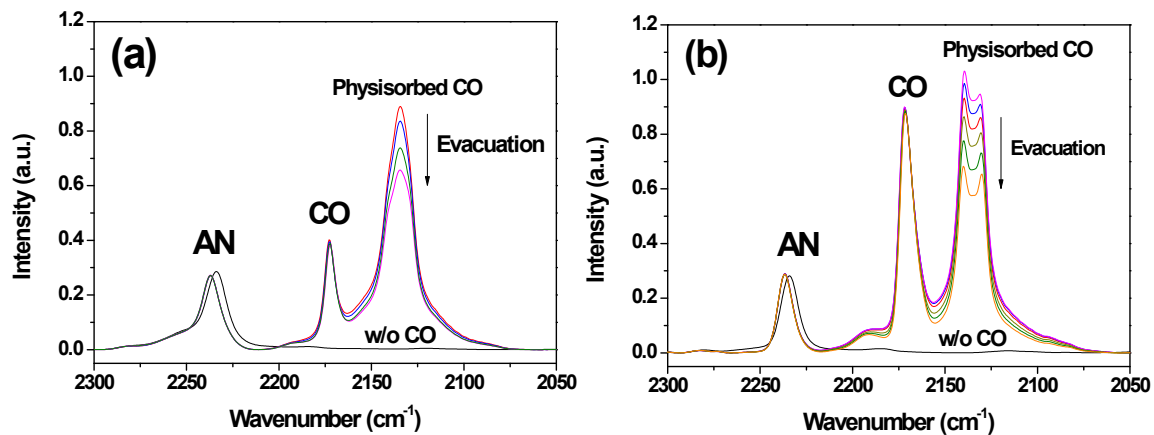


Figure S11. FT-IR spectra of (a) $\text{Cu}_3(\text{BTC})_2$ and (b) $\text{O-POSS}@Cu_3(\text{BTC})_2$ at 110 K. Samples were thermally treated at 423 K for 12 h before the IR experiment. Amino-5-nitrobenzonitrile (AN) was used as an internal standard to make self-supported wafers.

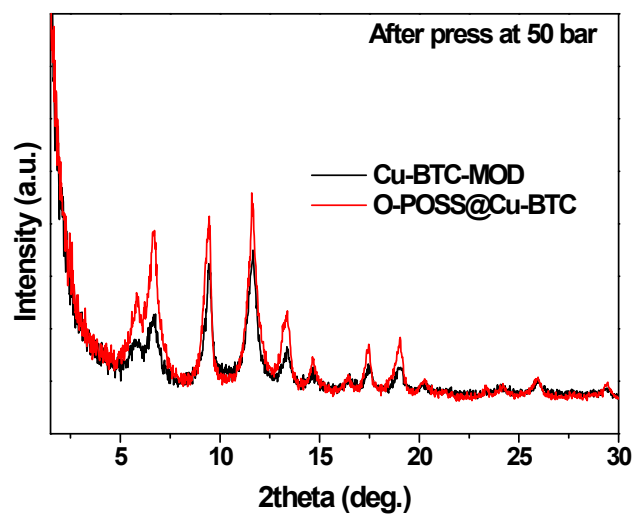


Figure S12. XRD patterns of (a) $\text{Cu}_3(\text{BTC})_2$ and (b) $\text{O-POSS@Cu}_3(\text{BTC})_2$ after IR experiment.

Ammonia adsorption

Removal of toxic gases, particularly ammonia, have generated considerable research interest.¹ In order to determine the ammonia sorption capacity, breakthrough test were performed at room Temperature. Breakthrough curve and adsorption capacities of NH₃ for RH 15% condition are presented in Figure S13 and in Table S1. Surprisingly, normalized sorption capacity is almost the same in both Cu₃(BTC)₂ and O-POSS@Cu₃(BTC)₂, in spite of different surface areas. As expected, O-POSS@Cu₃(BTC)₂ showed higher amounts of ammonia adsorption capacity compared to Cu₃(BTC)₂ in the reactivated samples (Fig S14 and Table SI). However, the crystallinity of CuBTC was completely lost during the NH₃ breakthrough test at RH 15%, while the crystal structure remained in O-POSS@Cu₃(BTC)₂ (Fig. S15). From this result, it can be conclude that POSS-modified crystal is less attacked after NH₃ sorption. The higher ammonia sorption capacity of reactivated O-POSS@Cu₃(BTC)₂ relative to the reactivated Cu₃(BTC)₂ may be due to the increased water stability in the presence of ammonia in a wet condition.

- (a) J. F. Van Humbeck, T. M. McDonald, X. Jing, B. M. Wires, G. Zhu and J. R. Long, *J. Am. Chem. Soc.*, 2014, **136**, 2432; (b) J. B. Decoste and G. W. Peterson, *Chem. Rev.*, 2014, **114**, 5695.

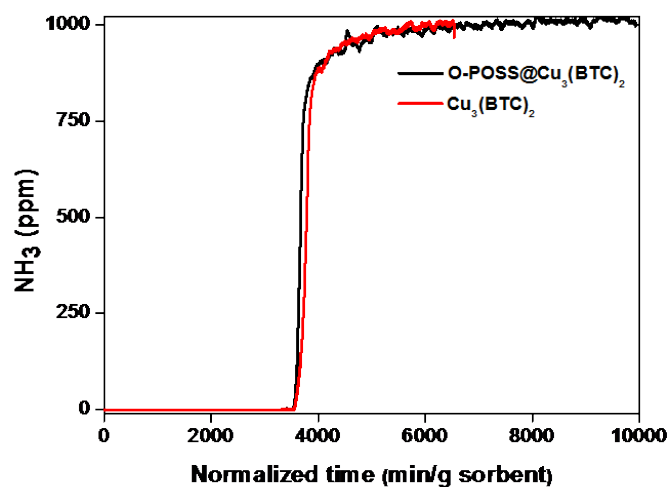


Figure S13. NH₃ breakthrough curves of Cu₃(BTC)₂ and O-POSS@Cu₃(BTC)₂ under 15 % RH condition.

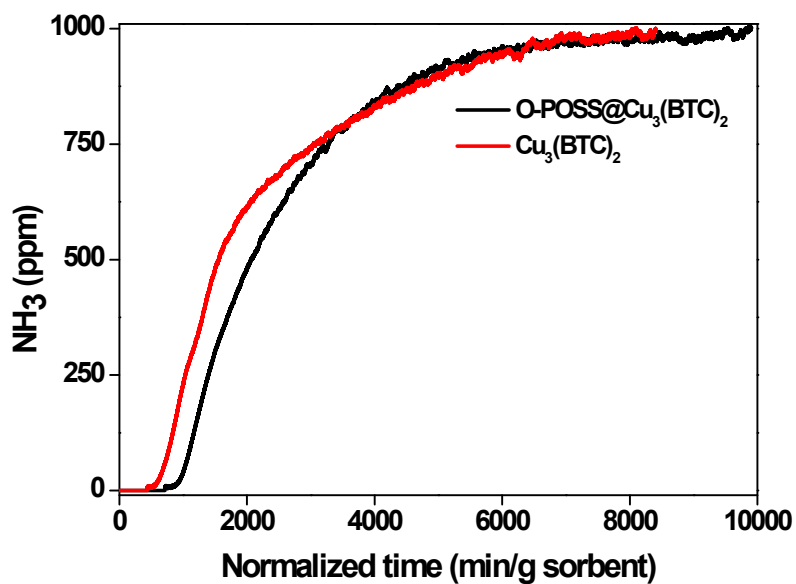


Figure S14. NH_3 breakthrough curves of reactivated $\text{Cu}_3(\text{BTC})_2$ and $\text{O-POSS@Cu}_3(\text{BTC})_2$, under 15 % RH condition.

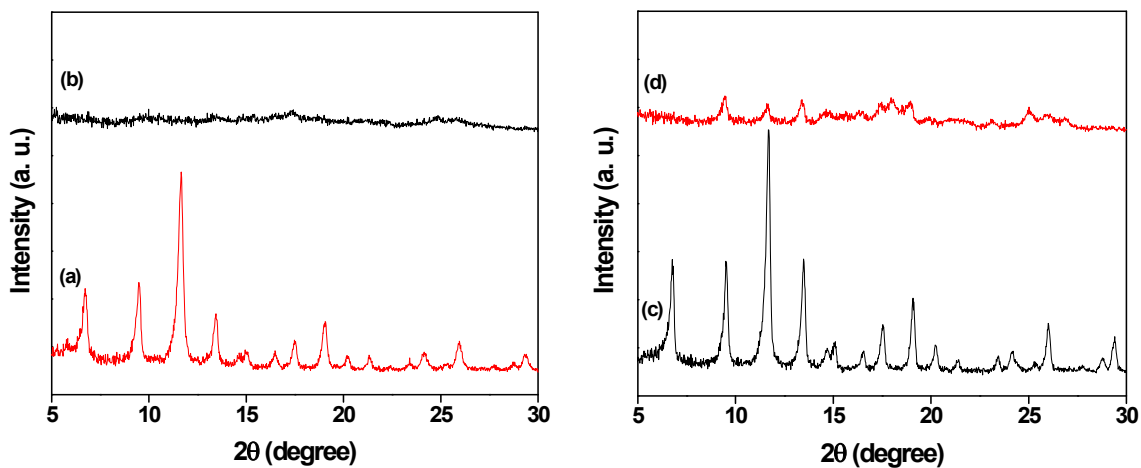


Figure S15 Comparison of the XRD patterns of $\text{Cu}_3(\text{BTC})_2$ and $\text{O-POSS@Cu}_3(\text{BTC})_2$, before (a and c) and after (b and d) NH_3 sorption under 15 % RH condition respectively.

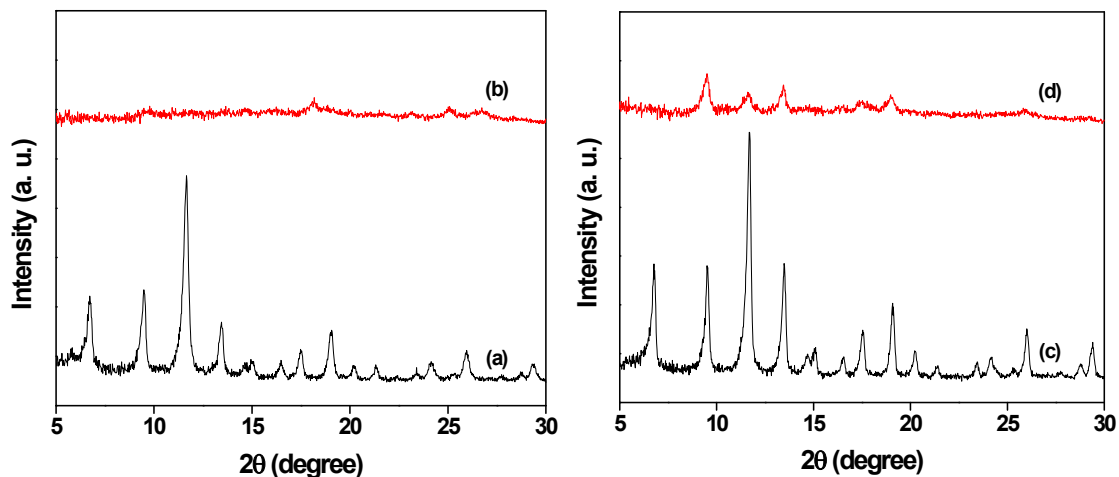


Figure S16 Comparison of the XRD patterns of $\text{Cu}_3(\text{BTC})_2$ and $\text{O-POSS}@Cu_3(\text{BTC})_2$, before (a and c) and after (b and d) NH_3 sorption under dry condition respectively.

From the XRD patterns of $\text{Cu}_3(\text{BTC})_2$ and $\text{O-POSS}@Cu_3(\text{BTC})_2$ after NH_3 sorption under dry condition, it can be seen that the crystal structure is remained in the $\text{O-POSS}@Cu_3(\text{BTC})_2$, whereas the structure of $\text{Cu}_3(\text{BTC})_2$ collapsed completely. From the above results it can be concluded that the structure loss is mainly due to NH_3 .

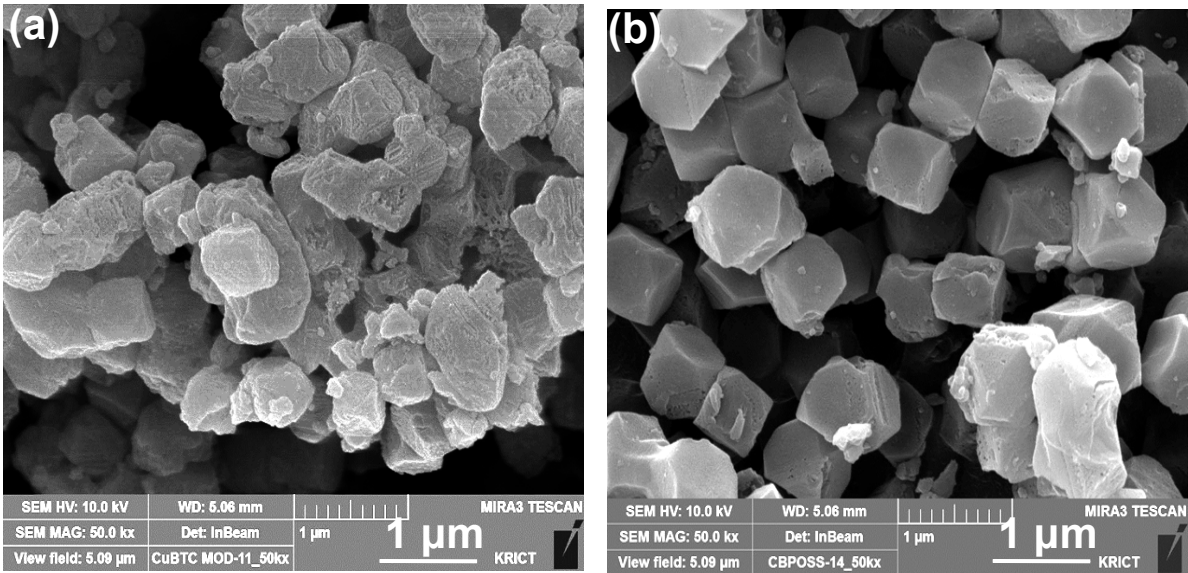


Figure S17 Comparison of the SEM images of (a) $\text{Cu}_3(\text{BTC})_2$ and (b) $\text{O-POSS}@Cu_3(\text{BTC})_2$ after NH_3 sorption under 15 % RH condition.

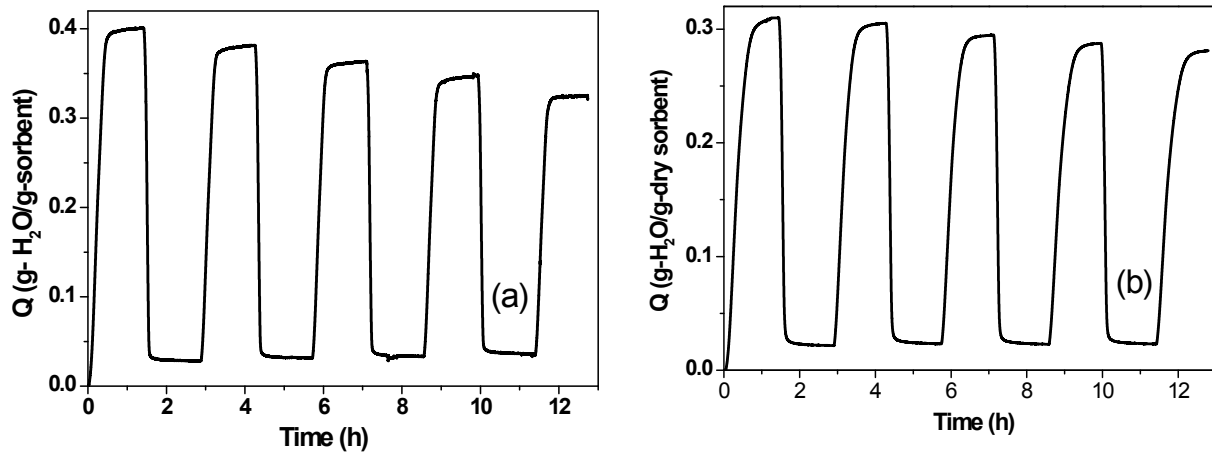


Figure S18. Dynamic water adsorption-desorption cycle test of (a) $\text{O-POSS}@Cu\text{BTC}$ and (b) $\text{PDMS}@Cu\text{BTC}$.